ARTICLE   OPEN

Broken rotational symmetry on the Fermi surface of a high-T$_c$ superconductor

B. J. Ramshaw[1,6], N. Harrison[1], S. E. Sebastian[2], S. Ghannadzadeh[3,7], K. A. Modic[1,8], D. A. Bonn[4], W. N. Hardy[4], Ruixing Liang[4] and P. A. Goddard[5]

Broken fourfold rotational (C$_4$) symmetry is observed in the experimental properties of several classes of unconventional superconductors. It has been proposed that this symmetry breaking is important for superconducting pairing in these materials, but in the high-T$_c$ cuprates this broken symmetry has never been observed on the Fermi surface. Here we report a pronounced anisotropy in the angle dependence of the interlayer magnetoresistance of the underdoped high transition temperature (high-T$_c$) superconductor YBa$_2$Cu$_3$O$_{6.58}$, directly revealing broken C$_4$ symmetry on the Fermi surface. Moreover, we demonstrate that this Fermi surface has C$_2$ symmetry of the type produced by a uniaxial or anisotropic density-wave phase. This establishes the central role of C$_4$ symmetry breaking in the Fermi surface reconstruction of YBa$_2$Cu$_3$O$_{6+\delta}$, and suggests a striking degree of universality among unconventional superconductors.

npj Quantum Materials (2017)2:8 ; doi:10.1038/s41535-017-0013-z

INTRODUCTION

Broken C$_4$ symmetry is observed in a number of experiments on unconventional superconductors, including transport,[1–4] nuclear magnetic resonance (NMR),[5, 6] neutron scattering,[7, 8] X-ray scattering[9–11] and scanning tunneling microscopy.[12, 13] In the iron-based superconductors broken C$_4$ symmetry is observed directly on the Fermi surface,[14] and has been taken as an indication that this broken symmetry drives the high T$_c$.[15] The question of whether the same type of symmetry breaking is relevant in the copper-oxide high-T$_c$ superconductors[16] has been left open because it has never been observed on the Fermi surface.[17, 18] Without a link to the Fermi surface, it is hard to make a compelling argument that the experimental observations of broken C$_4$ symmetry are relevant to the phenomenon of high-T$_c$.

The Fermi surface of a metal is constrained by the symmetry of its electronic environment. A precise determination of Fermi surface geometry, therefore, provides information about symmetry-breaking states of matter that feed back into the electronic structure. In the underdoped high-T$_c$ cuprates it is now well established that a charge-density wave (CDW) competes with superconductivity, but a direct experimental connection is still missing between the CDW and the Fermi surface. QO (quantum oscillation) measurements, performed in the high-field state, have been instrumental in determining the presence of a small electron Fermi surface in the underdoped side of the phase diagram.[17, 19–22] While QOs provide precise information about the area of the Fermi surface, they are relatively insensitive to its overall shape in two-dimensional (2D) metals (e.g., circular vs. square in cross-section). Here, we present the results of a complementary technique, angle-dependent magnetoresistance (AMR), that determines the geometry and symmetry of the Fermi surface. We identify the shape of the Fermi surface as consistent with certain proposed CDW reconstruction scenarios,[17, 23–27] and we find that this reconstruction is anisotropic in nature.

RESULTS

Since the 1930s it has been known that a change in resistance with an applied magnetic field—magnetoresistance—provides geometric information about a metallic Fermi surface,[28] and early magnetoresistance experiments were instrumental in developing the modern quantum theory of metals.[29] Real metals have non-spherical Fermi surfaces, thus magnetoresistance can be a strong function of the angle between the magnetic field and the crystal axes, giving rise to AMR. The signatures of AMR are particularly strong for quasi-2D Fermi surfaces, and thus this technique is well suited for determining the Fermi surface geometry of the high-T$_c$ cuprates.[30–34] To map the Fermi surface geometry of YBa$_2$Cu$_3$O$_{6.58}$ we performed interlayer (ρ_{zz}) magnetoresistance measurements in a fixed magnetic field of 45 T even in the absence of interlayer-coherence, AMR is still sensitive to the Fermi surface geometry (see ref. [35]). The field-angle dependence of ρ_{zz} was obtained by rotating the sample in situ, sweeping the polar angle θ between the magnetic field and the crystalline ĉ-axis for several values of the azimuthal angle ϕ (see the inset of Fig. 1a for angle definitions). Our primary observation is twofold anisotropy of the AMR as a function of ϕ—immediately apparent in Fig. 1—with the AMR increasing much more rapidly on rotating the field

[1]Los Alamos National Labs, Los Alamos, NM, USA; [2]Cavendish Laboratory, Cambridge University, Cambridge CB3 OHE, UK; [3]High Field Magnet Laboratory, Radboud University, 6525 ED Nijmegen, The Netherlands; [4]University of British Columbia, Vancouver, Canada and [5]Department of Physics, University of Warwick, Gibbet Hill Road, Coventry CV4 7AL, UK
Correspondence: B. J. Ramshaw (bradramshaw@cornell.edu)
[6]Present address: Laboratory of Atomic and Solid State Physics, Cornell University, Ithaca, NY 14853, USA
[7]Present address: Oxford Instruments NanoScience, Tubney Woods, Abingdon, Oxfordshire OX13 5QX, UK
[8]Present address: Max-Planck-Institute for Chemical Physics of Solids, Noethnitzer Strasse, Dresden 40, Germany

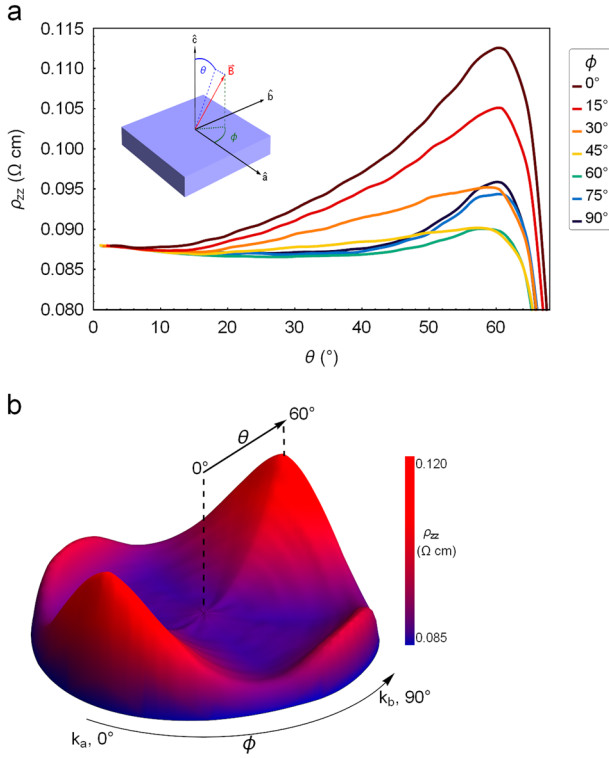**Fig. 1** The angle-dependent magnetoresistance of YBa$_2$Cu$_3$O$_{6.58}$. The raw resistance (**a**) as a function of θ at 45 T and 15 K, for several values of ϕ spanning between the â-axis ($\phi = 0°$) and b̂-axis ($\phi = 90°$). The rapid drop in resistivity beyond $\theta = 60°$ is due to the onset of superconductivity when insufficient magnetic field is parallel to the ĉ-axis. The inset defines the field angles ϕ and θ with respect to the crystallographic â, b̂, and ĉ axes. This data was taken at a temperature of 15 K to increase the polar angular range over which the normal resistive state is accessed,[64] and to thermally suppress QOs. Broken C$_4$ symmetry is clearly shown in a polar plot of the data **b**, where the radius is the polar angle θ, and the amplitude and color correspond to the magnitude of the resistance

towards the crystalline â-axis ($\phi = 0°$) than towards the b̂-axis ($\phi = 90°$). As we demonstrate below, this directly indicates that Fermi surface has strongly broken C$_4$ symmetry.

In order to understand the connection between AMR and the Fermi surface, we first perform a qualitative analysis of the three most salient features in the data: C$_2$ symmetry; negative AMR at low θ near the $\phi = 90°$ directions; and suppression of AMR along the $\phi = 90°$ direction at high θ. The semi-classical conductivity of a metal is given by the velocity-velocity correlation function of all quasiparticles on the Fermi surface, averaged over their lifetime τ.[36, 37] Magnetoresistance arises because the quasiparticle velocity —which is always perpendicular to the Fermi surface—is altered by the Lorentz force, which induces cyclotron motion perpendicular to the magnetic field (see Fig. 2a for a schematic cyclotron orbit). If τ is sufficiently long, orbiting quasiparticles sample a significant portion of the Fermi surface perimeter before scattering. Depending on the specific geometry of the cyclotron orbit, components of the quasiparticle velocity (v_z, for example) may average to zero, resulting in a vanishingly small contribution to the conductivity for that field direction. The total magnetoresistance at a particular field orientation is then given by the ensemble of all quasiparticle orbits on the Fermi surface at that angle, and AMR, therefore, encodes the Fermi surface geometry.

Underdoped YBa$_2$Cu$_3$O$_{6+\delta}$ contains, at a minimum, two sections of Fermi surface due to its bilayer crystal structure (Fig. 3a). The phenomenon of magnetic breakdown, whereby quasiparticles in a magnetic field can jump between Fermi surfaces separated by small energy gaps,[38] leads to multiple possible cyclotron orbits for the reconstructed Fermi surface of YBa$_2$Cu$_3$O$_{6.58}$ (refs 17, 39, 40). For the purpose of simulating our AMR, we calculate the conductivity for each breakdown path separately and then sum the conductivities in parallel. In general, the interlayer dispersion of a quasi-2D Fermi surface—which determines the interlayer resistivity ρ_{zz}—can be expanded in cylindrical harmonics, three of which are shown in Fig. 2b. The simplest harmonic $\cos k_z$ produces magnetoresistance that increases with θ for all ϕ. The harmonic $\sin 2\phi \cos k_z$ produces fourfold symmetric AMR that decreases with increasing θ, with a weaker effect along the diagonal directions. The simplest harmonic to break C$_4$ symmetry in the interlayer tunneling is $\sin 2\phi \cos k_z$, which has twofold symmetry and gives
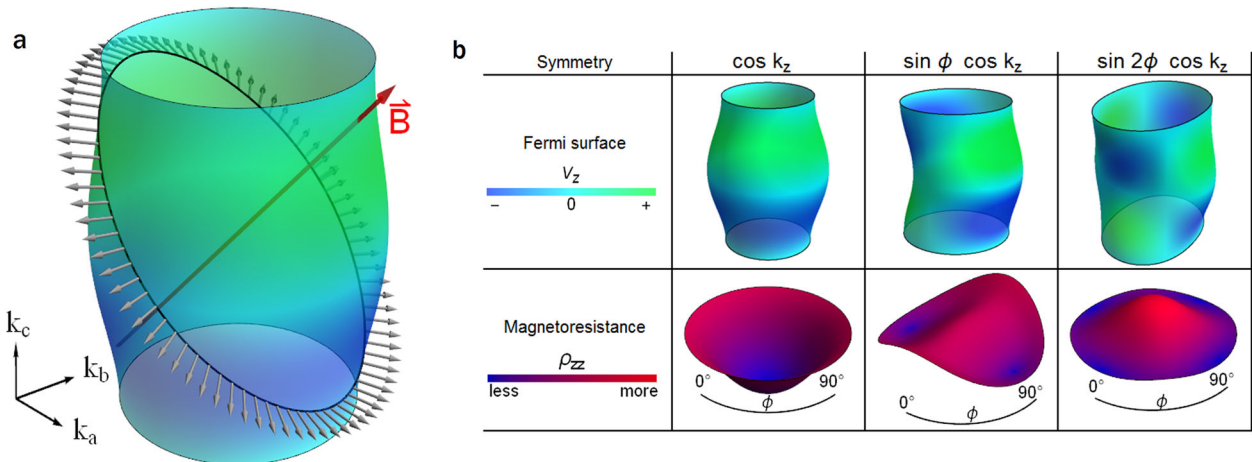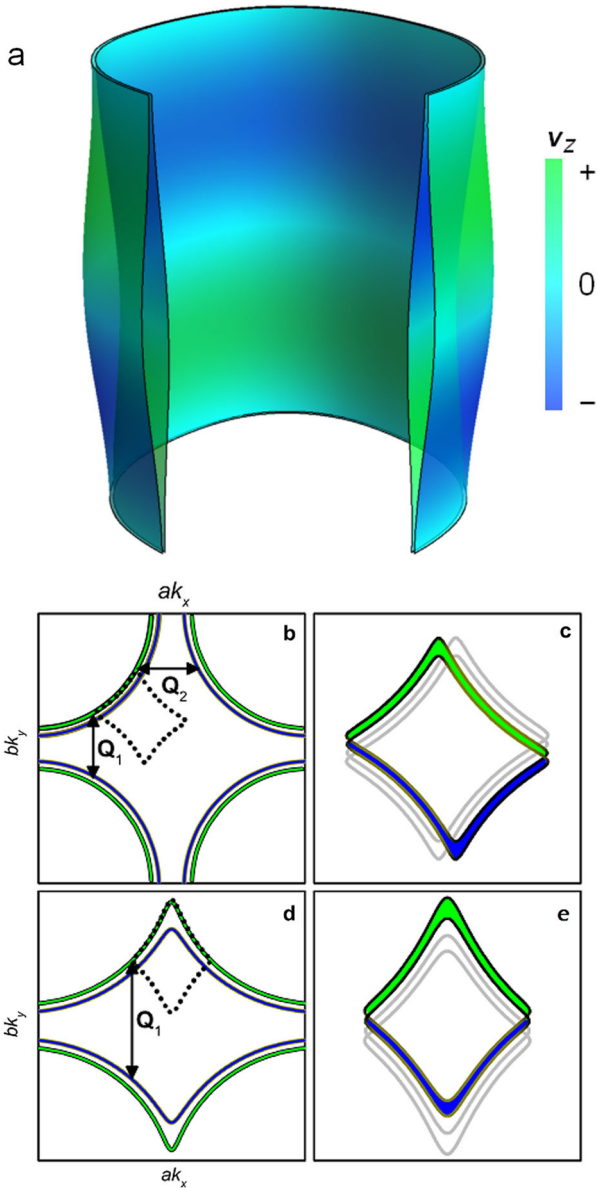

Fig. 2 Quasiparticle trajectory and magnetoresistance for different interlayer tunneling symmetries. Schematic Fermi surface with a cyclotron orbit. **a** Quasiparticles experience a Lorentz force in a magnetic field (*red arrow*), inducing cyclotron motion perpendicular to the field direction. *Gray arrows* indicate the Fermi velocity along a cyclotron orbit (*black line*). Dispersion along the k_z direction modulates the ẑ component of the velocity and changes the sign of v_z around the cyclotron orbit. Panel **b** shows the three dominant ĉ-axis dispersion shapes allowed by symmetry in YBa$_2$Cu$_3$O$_{6.58}$ (*top panels*) and their subsequent contributions to the AMR (*bottom panels*). Full rotational symmetry is preserved for the $\cos k_z$ dispersion, while $\sin\phi \cos k_z$ has C$_2$ symmetry. $\sin 2\phi \cos k_z$ has C$_2$ symmetry but produces C$_4$ symmetric AMR once all cyclotron orbits are accounted for. For clarity we have presented these Fermi surfaces with isotropic k_F to emphasize the symmetry of the warping: in Fig. 4a these warpings will be superimposed on the actual diamond-like k_F that we obtain from modeling the AMR

Fig. 3 Two possible anisotropic CDW reconstruction schematics forYBa$_2$Cu$_3$O$_{6.58}$. The unreconstructed cuprate Fermi surface is a large hole-like cylinder.[18,32,65] **a** The bilayer copper oxide planes of YBa$_2$Cu$_3$O$_{6+\delta}$ give rise to bonding and anti-bonding bands, whose interlayer velocities have opposite signs (one quarter of the Fermi surface has been cut away for clarity). The right hand panels are projections of this surface into the k_a–k_b plane, from $k_z = -\pi/c$ to $k_z = 0$, before (**b** and **d**) and after (**c** and **e**) Fermi surface reconstruction. The color scale signifies the sign of v_z. The *upper* two panels involve two anisotropic CDWs, with $Q_2 = (\delta, 0, 1/2)$ and $Q_2 = (\delta, 0, 0)$ (refs 9, 11, 58), whereas the *bottom* two panels are the result of a large nematic distortion.[59] followed by uni-axial CDW reconstruction with $Q_2 = (\delta, 0, 0)$, and where $\delta \approx 0.3$ according to X-ray scattering measurements.[9] Multiple Fermi surface sections, between which magnetic breakdown is possible,[17,24,39,40] are present after reconstruction: for clarity we color only one section

AMR that decreases with increasing θ along one ϕ direction and very weak AMR along the perpendicular direction. The measured twofold anisotropy of ρ_{zz} in YBa$_2$Cu$_3$O$_{6.58}$, along with the negative AMR at low θ near the $\phi = 90°$ directions, therefore, suggests that there is a significant contribution from a section of Fermi surface with $\sin\phi\cos k_z$ symmetry. The most obvious reason for the

existence of such a symmetry-breaking Fermi surface inYBa$_2$Cu$_3$O$_{6.58}$ is if the Fermi surface reconstruction itself breaks C$_4$ symmetry—the unreconstructed Fermi surface of YBa$_2$Cu$_3$O$_{6+\delta}$ is only slightly distorted from C$_4$ symmetry by the weakly orthorhombic crystal structure.[41] While the crystal structure of YBa$_2$Cu$_3$O$_{6+\delta}$ inherently breaks C$_4$ symmetry, we argue that the small symmetry-breaking strain field arising from the orthorhombicity serves to preferentially align an underlying electronic instability.[3] Our simulations suggest that anisotropy in the scattering rate; anisotropy in the interlayer hopping that is still finite in all directions; or an in-plane anisotropy in the Fermi wavevector (i.e., a Fermi surface elongated along one in-plane direction), cannot produce magnetoresistance with the angular structure we observe (see Supplementary Information for details).

Another prominent feature in the data is the suppression of AMR along the $\phi = 45°$ direction, particularly above $\phi = 50°$. In addition to the interlayer velocity, AMR is responsive to the in-plane geometry of the Fermi surface.[30–34, 42] For a cylindrical surface with simple $\cos k_z$ warping and an isotropic Fermi radius k_F (see Fig. 2b), the AMR evolves with field angle θ as $\rho_{zz}(\theta) \propto 1/(J_0(k_F c \tan\theta))^2$, where c is the ĉ-axis lattice constant (see footnote for more complicated warping geometries the actual form of $\rho_{zz}(\theta)$ is different, but it is still the product $k_F c$ that sets the angular scale over which the maxima in ρ_{zz} appear). The AMR shows maxima wherever $k_F c \tan(\theta)$ equals a zero of the Bessel function J_0, which happens for certain "Yamaji" angles where the interlayer velocity averages to zero around the cyclotron orbit.[43] A critical feature of this form of ρ_{zz} is that the product $k_F c$ sets the scale in θ over which these maxima in ρ_{zz} appear: a smaller k_F pushes the resistance maxima out to higher angles. For quasi-2D Fermi surfaces that are non-circular in cross section (anisotropic $k_F(\phi)$), $k_F c$ still sets the angular scale, but to a first approximation it is $k_F(\phi_0)$—where ϕ_0 is the direction in which the magnetic field is being rotated—that determines where θ and ϕ the maxima in ρ_{zz} appear. For YBa$_2$Cu$_3$O$_{6.58}$ we can use the average value of $k_F \approx 1.27$ nm^{-1} determined by QOs to estimate that the first maximum in ρ_{zz} should appear around $\theta \approx 58°$. While this means that we cannot reach any AMR maxima before the onset of superconductivity, we are still able to observe the approach to the first maximum. The relatively weak AMR observed when the field is rotated in the $\phi = 45°$ direction suggests that the Fermi surface has a smaller k_F along the diagonals than along the â and b̂ axes— that its first maximum is pushed to higher θ. This points to a Fermi surface with a square or diamond-like in-plane geometry— strikingly similar to the Fermi surface reconstruction predicted to occur via CDW.[17, 23–27] Two scenarios that could give rise to this type of reconstruction are shown in Fig. 3.

We can now combine our qualitative Fermi surface information —interlayer tunneling with C$_2$ symmetry on at least one Fermi surface section, and an in-plane diamond shape—and quantitatively model our data by numerically solving the Boltzmann transport equation[36] (see Supplementary Information for details). To avoid over-parametrization of the data we model only the three $F = 530$ T "breakdown" surfaces (plus their symmetry-related copies), which are known to dominate the ĉ-axis conductivity.[44, 45] We fix the cross-sectional area of the orbits to the value of $A_k = 2\pi e/\hbar \cdot 530$ T ≈ 5.1 nm^{-2} obtained from QO measurements on YBa$_2$Cu$_3$O$_{6.58}$ (ref. 44), and allow a single value of τ to vary as a free parameter for all three surfaces. We find that the AMR is best modeled by a sum of 41% of a surface with $\sin\phi\cos k_z$ symmetry, 27% of a surface with $\cos k_z$ symmetry, and 32% of a surface with $\sin 2\phi\cos k_z$ symmetry. These proportions are reasonably in line with what is expected from the number of possible breakdown orbits and their magnetic breakdown probabilities.[17] In Fig. 4 we show that the most important features of the AMR which we first identified on qualitative grounds—C$_2$ symmetry, negative AMR near $\phi = 90°$, and suppression along the ($\phi = 45°$) direction at high θ—are captured by this model. It is important to note that
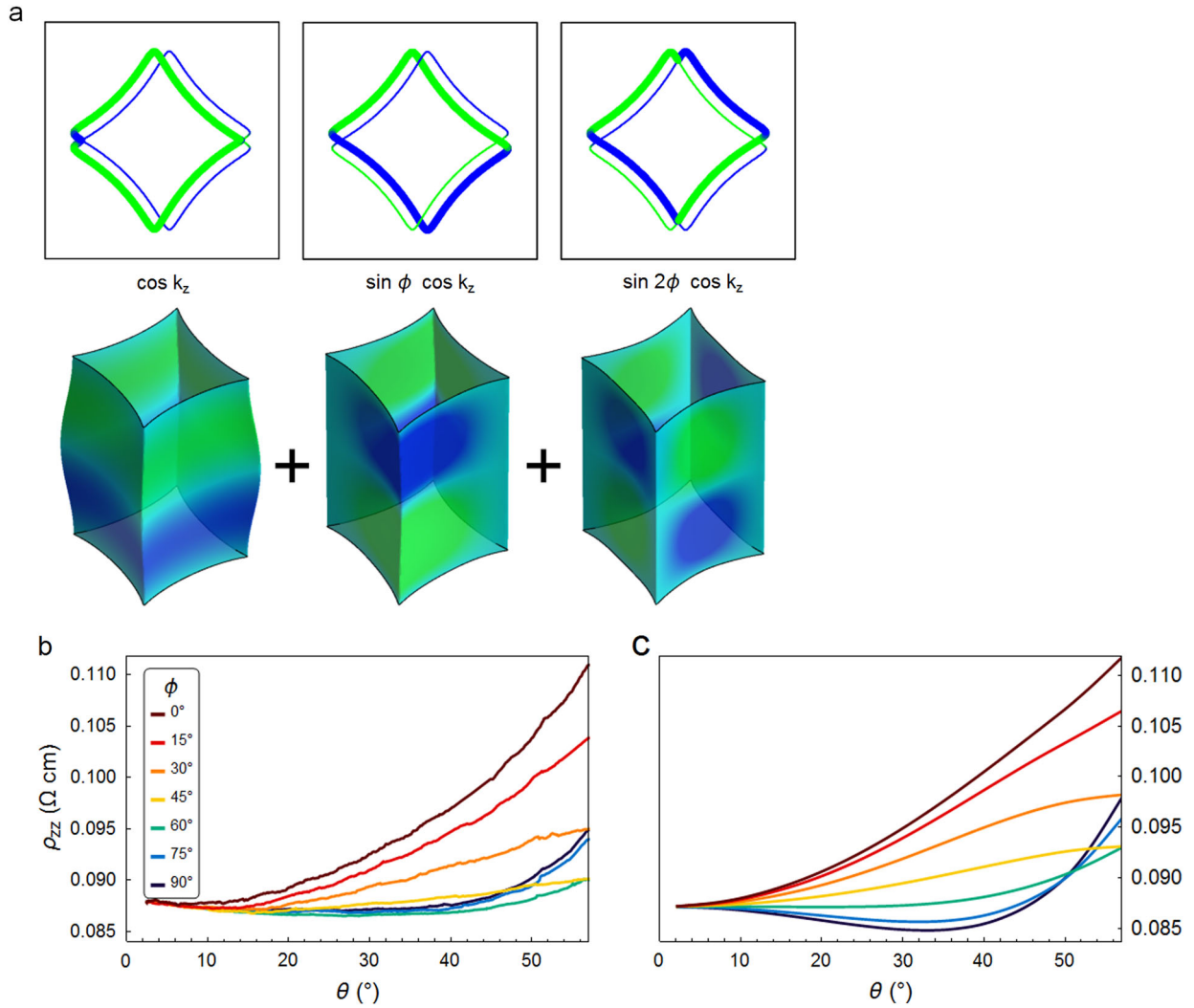
a

Fig. 4 Simulated magnetoresistance from a single bilayer-split pocket in$YBa_2Cu_3O_{6.58}$. The model Fermi surface consists of three dominant breakdown sections (**a**) that combine the in-plane diamond geometry of Fig. 3 with the interlayer dispersion symmetries of Fig. 2b (which were shown with isotropic k_F to emphasize their symmetry). The raw magnetoresistivity data is reproduced in panel **b**, truncated at $\theta = 58°$ at the onset of superconductivity. Panel **c** is a simulation of this data using the three magnetic breakdown orbits contributing to the dominant QO frequency, which have symmetries shown in Fig. 2b. The strongest contribution comes from the cylinder with $\sin\phi \cos k_z$ warping, which explains the dominant C_2 symmetry we observe in the AMR

resistivity is not a linear function of the interlayer hopping parameters: combining all three symmetry warpings onto a single section of Fermi surface cannot reproduce the data.

The consistency between our Fermi surface model and other experiments can now be checked. The quasiparticle lifetime we extract from the simulations is $\tau = 0.24 \pm 0.05$ ps—in agreement with the 0.27 ps reported from QOs.[46] Zero-field resistivity measurements at this doping find an in-plane resistive anisotropy that is collapsing towards one at low temperatures: this behavior is attributed to the conductivity of the 1D copper-oxide chains freezing out at low temperature.[2] Our model, which breaks C_4 symmetry only in the $\hat{c}$-axis dispersion of the Fermi surface, naturally preserves the near-isotropy of the $\hat{a}$-$\hat{b}$-plane conductivity. If the 1D copper oxide chain layer were clean enough to produce AMR—and there are is evidence from spectroscopy to believe that this is not the case[47–49]—then the resultant in-plane resistivity would be highly anisotropic: such in-plane anisotropy is not observed experimentally.[2] AMR from an open Fermi surface produced by the chain layer would also not produce the observed

upturn in the AMR we observe above $\theta = 40°$ when $\phi = 90°$(see Supplementary Information for details). AMR measurements can detect sections of Fermi surface that are invisible to QOs, such as open sheets and surfaces with higher scattering rates (shorter τ). AMR, therefore, has the potential to observe sections of Fermi surface in $YBa_2Cu_3O_{6.58}$ formed by CDW reconstruction that have remained unobserved by QOs. Our simulation reveals, however, that the AMR can be fully accounted for by the same bilayer-split electron pocket that appears in QO experiments, with no additional sheets or pockets. This is consistent with previous suggestions that there is only a single Fermi pocket in the Brillouin zone of underdoped $YBa_2Cu_3O_{6+\delta}$ (refs 50, 51). We note that the small hole pocket reported at this doping[52] has a cross-section (k_F) that is too small to contribute any significant AMR below $\theta \approx 75°$, thus we do not include the possibility of this surface in our model.

It is important to note that our model relies on the validity of the single-particle picture and Boltzmann transport equations. While these assumptions may be valid for the small Fermi pocket we observe—and the observation of the same pocket via QOs

strongly suggests this to be true[53]—there is much experimental evidence that large portions of the Fermi surface exhibit decidedly *non*-quasiparticle behavior.[54] This includes the linear-in-temperature zero-field resistivity above the pseudogap temperature.[55–57] One possibility is that high magnetic fields suppress the pseudogap and restore the entire Fermi surface to a Fermi-liquid state—the possible Fermi surface reconstruction presented in Fig. 3d, e would require such a scenario for the pocket near the anti-nodal region to be ungapped. This possibility suffers from the fact that no other pieces of Fermi surface besides the small electron pocket are observed in high magnetic fields. Despite the apparent ability of single-particle Boltzman equations to model the high-field magneotransport, it remains an important open question as to how to connect the zero-field metallic state to that observed in high magnetic fields.

DISCUSSION

In order to obtain a Fermi surface with C_2 symmetry from the C_4 symmetric unreconstructed Fermi surface,[41] the mechanism of Fermi surface reconstruction must itself break C_4 symmetry. We suggest that the diamond-like shape we measure with AMR strongly constrains the reconstruction scenario to one of density-wave origin. There is experimental evidence for broken C_4 symmetry in the CDW: NMR measurements to 28.5 T are consistent with a high-field unidirectional CDW ("stripe") phase,[5] and recent X-ray measurements indicate that the CDW modulated along the $\hat{b}$-axis —which has the same wavevector as the CDW modulated along the $\hat{a}$-axis in zero field—acquires a new $\hat{c}$-axis component above 15 T (refs 11, [58]). We suggest that this asymmetry in the $\hat{c}$-axis components of the wavevectors persists to at least 45 T, and that these CDWs are responsible for the Fermi surface reconstruction, as has been proposed theoretically.[17, 23–27] A second route to a diamond-like pocket with C_2 symmetry in the $\hat{c}$-axis tunneling requires a strong nematic distortion of the Fermi surface (see Fig. 3d, e).[59] In high magnetic fields this surface is then reconstructed by a unidirectional CDW. This scenario only requires the single CDW wavevector that acquires three-dimensional coherence in high fields.[11, 58]

Independent of the specific model, our analysis shows that Fermi surface reconstruction in $YBa_2Cu_3O_{6.58}$ is anisotropic, and that the entire AMR signature can be accounted for by the same Fermi surface that is responsible for QOs and a negative Hall coefficient in high magnetic fields. We have also established that although the CDW in the cuprates is relatively weak and disordered compared to more traditional CDW metals,[60] its symmetry and wavevector directly determine Fermi surface properties. This is similar to the iron pnictide superconductors, where the nematic state is directly observable on the Fermi surface,[14] and suggests that the physics underlying both the superconductivity and the quantum criticality in these two classes of materials share a similar origin. Our Fermi surface model predicts that for tetragonal $HgBa_2CuO_4$, where both short-range CDW order and a small Fermi surface have been observed,[61, 62] sufficient uniaxial strain should favour anisotropic CDW formation and give rise to anisotropic AMR similar to what we have observed in $YBa_2Cu_3O_{6.58}$.

METHODS

Detwinned single crystals of $YBa_2Cu_3O_{6.58}$ were grown and prepared as described in Liang et al.[63] C-axis contacts were prepared as described in Ramshaw et al.[44] Resistivity measurements were conducted in the 45 Tesla hybrid magnet at the National High Magnetic Field Lab in Tallahassee using a 2-axis rotator. The resistance was measured with a 4-point contact geometry using an SRS 830 lockin amplifier: the sample was driven with $I = 500\,\mu A$ at a frequency of $f = 37.7$ Hz.

AUTHOR CONTRIBUTIONS

S.G., P.A.G., N.H., B.J.R, and S.E.S. performed the 45 Tesla AMR measurements at the NHMFL in Tallahassee, Florida. B.J.R and K.A.M. performed additional sample characterization at the NHMFL in Los Alamos, New Mexico. D.A.B., W.N.H, R.L., and B.J.R. grew and prepared the $YBa_2Cu_3O_{6.58}$ samples. N.H. and B.J.R. performed the data analysis and wrote the manuscript with input from all co-authors.

COMPETING INTERESTS

The authors declare no competing interests.

REFERENCES

1. Borzi, R. et al. Formation of a nematic fluid at high fields in Sr3Ru2O7. *Science* **315**, 214–217 (2007).
2. Ando, Y., Segawa, K., Komiya, S. & Lavrov, A. N. Electrical resistivity anisotropy from self-organized one dimensionality in high-temperature superconductors. *Phys. Rev. Lett.* **88**, 137005 (2002).
3. Daou, R. et al. Broken rotational symmetry in the pseudogap phase of a high-Tc superconductor. *Nature* **463**, 519–522 (2010).
4. Chu, J.-H. et al. In-plane resistivity anisotropy in an underdoped iron arsenide superconductor. *Science.* **329**, 824–826 (2010).
5. Wu, T. et al. Magnetic-field-induced charge-stripe order in the high-temperature superconductor YBa2Cu3Oy. *Nature* **477**, 191–194 (2011).
6. Wu, T. et al. Incipient charge order observed by NMR in the normal state of YBa2Cu3Oy. *Nat. Commun.* **6**, 6438 (2015).
7. Stock, C. et al. Dynamic stripes and resonance in the superconducting and normal phases of $YBa_2Cu_3O_{6.5}$ ortho-II superconductor. *Phys. Rev. B* **69**, 014502 (2004).
8. Hinkov, V. et al. Electronic liquid crystal state in the high-temperature superconductor YBa2Cu3O6.45. *Science* **319**, 597–600 (2008).
9. Blanco-Canosa, S. et al. Resonant x-ray scattering study of charge density wave correlations in Yba_2Cu_3O6+x. *arXiv preprint arXiv:1406.1595*(2014).
10. Comin, R. et al. Broken translational and rotational symmetry via charge stripe order in underdoped YBa2Cu3O6+y. *Science* **347**, 1335–1339 (2015).
11. Chang, J. et al. Magnetic field controlled charge density wave coupling in underdoped $Yba_2Cu_3O_{6+x}$. *arXiv preprint arXiv:1511.06092* (2015).
12. Howald, C., Eisaki, H., Kaneko, N., Greven, M. & Kapitulnik, A. Periodic density-of-states modulations in superconducting Bi2Sr2CaCu2O8+δ. *Phys. Rev.B* **67**, 014533 (2003).
13. Kohsaka, Y. et al. An intrinsic bond-centered electronic glass with unidirectional domains in underdoped cuprates. *Science* **315**, 1380–1385 (2007).
14. Nakayama, K. et al. Reconstruction of band structure induced by electronic nematicity in an FeSe superconductor. *Phys. Rev. Lett.* **113**, 237001 (2014).
15. Fernandes, R., Chubukov, A. & Schmalian, J. What drives nematic order in iron-based superconductors? *Nat. Phys.* **10**, 97–104 (2014).
16. Kivelson, S., Fradkin, E. & Emery, V. Electronic liquid-crystal phases of a doped Mott insulator. *Nature* **393**, 550–553 (1998).
17. Sebastian, S. E. et al. Normal-state nodal electronic structure in underdoped high-Tc copper oxides. *Nature* **511**, 61–64 (2014).
18. Hossain, M. A. et al. In situ doping control of the surface of high-temperature superconductors. *Nat. Phys.* **4**, 527–531 (2008).
19. Doiron-Leyraud, N. et al. Quantum oscillations and the fermi surface in an underdoped high-Tc superconductor. *Nature* **447**, 565–568 (2007).
20. LeBoeuf, D. et al. Electron pockets in the fermi surface of hole-doped high-Tc superconductors. *Nature* **450**, 533–536 (2007).
21. Singleton, J. et al. Magnetic quantum oscillations in YBa2Cu3O6.61 and YBa2-Cu3O6.69 in fields of up to 85 T: Patching the hole in the roof of the superconducting dome. *Phys. Rev. Lett.* **104**, 086403 (2010).

22. Ramshaw, B. J. *et al.* Quasiparticle mass enhancement approaching optimal doping in a high-Tc superconductor. *Science* **348**, 317–320 (2015).

23. Harrison, N. & Sebastian, S. E. Protected nodal electron pocket from multiple-Q in underdoped high temperature superconductors. *Phys. Rev. Lett.* **106**, 226402 (2011).

24. Harrison, N. & Sebastian, S. E. Fermi surface reconstruction from bilayer charge ordering in the underdoped high temperature superconductor YBa2Cu3O6+x. *New. J. Phys.* **14**, 095023 (2012).

25. Maharaj, A. V., Hosur, P. & Raghu, S. Crisscrossed stripe order from interlayer tunneling in hole-doped cuprates. *Phys. Rev. B* **90**, 125108 (2014).

26. Allais, A., Chowdhury, D. & Sachdev, S. Connecting high-field quantum oscillations to zero-field electron spectral functions in the underdoped cuprates. *Nat. Commun.* **5** (2014).

27. Briffa, A. K. R. *et al.* Fermi surface reconstruction and quantum oscillations in underdoped YBa2Cu3O7−x modeled in a single bilayer with mirror symmetry broken by charge density waves. *Phys. Rev. B* **93**, 094502 (2016).

28. Jones, H. & Zener, C. The theory of the change in resistance in a magnetic field. In *Proceedings of the Royal Society of London A: Mathematical, Physical and Engineering Sciences*, Vol. 145, 268–277 (The Royal Society, 1934).

29. Kapitza, P. The change of electrical conductivity in strong magnetic fields. Part I. Experimental results. *Proceedings of the Royal Society of London A: Mathematical, Physical and Engineering Sciences,* Vol. 123, 292–341 (1929).

30. Singleton, J. Studies of quasi-two-dimensional organic conductors based on BEDT-TTF using high magnetic fields. *Rep. Prog. Phys.* **63**, 1111 (2000).

31. Bergemann, C., Mackenzie, A., Julian, S., Forsythe, D. & Ohmichi, E. Quasi-two-dimensional fermi liquid properties of the unconventional superconductor Sr2RuO4. *Adv. Phys.* **52**, 639–725 (2003).

32. Hussey, N., Abdel-Jawad, M., Carrington, A., Mackenzie, A. & Balicas, L. A coherent three-dimensional fermi surface in a high-transition-temperature superconductor. *Nature* **425**, 814–817 (2003).

33. Analytis, J. G., Abdel-Jawad, M., Balicas, L., French, M. M. J. & Hussey, N. E. Angle-dependent magnetoresistance measurements in Tl2Ba2CuO6+δ and the need for anisotropic scattering. *Phys. Rev. B* **76**, 104523 (2007).

34. Kartsovnik, M. High magnetic fields: a tool for studying electronic properties of layered organic metals. *Chem. Rev.* **104**, 5737–5781 (2004).

35. Kennett, M. P. & McKenzie, R. H. Sensitivity of the interlayer magnetoresistance of layered metals to intralayer anisotropies. *Phys. Rev. B* **76**, 054515 (2007).

36. Chambers, R. The kinetic formulation of conduction problems. *Proceedings of the Physical Society of London Section A,* Vol. 65, 458–459 (1952).

37. Abrikosov, A. A. On the magnetic properties of superconductors of the second group. *Soviet Phys. JETP-USSR* **5**, 1174–1183 (1957).

38. Shoenberg, D. *Magnetic Oscillations in Metals. Cambridge Monographs on Physics* (Cambridge University Press, 1984).

39. Maharaj, A. V., Zhang, Y., Ramshaw, B. & Kivelson, S. Quantum oscillations in a bilayer with broken mirror symmetry: a minimal model for Yba2Cu3O6+δ. *arXiv preprint arXiv:1510.02116* (2015).

40. Forgan, E. *et al.* The microscopic structure of charge density waves in underdoped YBa2Cu3O6.54 revealed by X-ray diffraction. *Nat. Commun.* **6**, 10064 (2015).

41. Fournier, D. *et al.* Loss of nodal quasiparticle integrity in underdoped YBa2Cu3O6+x. *Nat. Phys.* **6**, 905–911 (2010).

42. Goddard, P. *et al.* Angle-dependent magnetoresistance of the layered organic superconductor $_{K^-}$(ET)(2)Cu(NCS)(2): Simulation and experiment. *Phys. Rev. B* **69**, 174509 (2004).

43. Yamaji, K. On the angle dependence of the magnetoresistance in quasi-2-dimensional organic superconductors. *J. Phys. Soc. Jpn.* **58**, 1520–1523 (1989).

44. Ramshaw, B. J. *et al.* Angle dependence of quantum oscillations in YBa2Cu3O6.59 shows free-spin behaviour of quasiparticles. *Nat. Phys.* **7**, 234–238 (2011).

45. Harrison, N., Ramshaw, B. J. & Shekhter, A. Nodal bilayer-splitting controlled by spin-orbit interactions in underdoped high-Tc cuprates. *Sci. Rep.* **5**, 10064 (2015).

46. Ramshaw, B. J. *Shubnikov-de Haas Measurements and the Spin Magnetic Moment of YBa$_2$Cu$_3$O6,95.* Ph.D. thesis, Univ. of British Columbia (2012).

47. Schlesinger, Z. *et al.* Superconducting energy gap and normal-state conductivity of a single-domain Yba$_2$Cu$_3$O$_7$ crystal. *Phys. Rev. Lett.* **65**, 801–804 (1990).

48. Basov, D. N. *et al.* Disorder and superconducting-state conductivity of single crystals of Yba$_2$Cu$_3$O$_{6.95}$. *Phys. Rev. B* **49**, 12165–12169 (1994).

49. Bobowski, J. S. *et al.* Oxygen chain disorder as the weak scattering source in Yba$_2$Cu$_3$O$_{6.50}$. *Phys. Rev. B* **82**, 134526 (2010).

50. Riggs, S. C. *et al.* Heat capacity through the magnetic-field-induced resistive transition in an underdoped high-temperature superconductor. *Nat. Phys.* **7**, 332–335 (2011).

51. Sebastian, S. E. *et al.* Chemical potential oscillations from nodal fermi surface pocket in the underdoped high-temperature superconductor YBa2Cu3O6+x. *Nat. Commun.* **2**, 471 (2011).

52. Doiron-Leyraud, N. *et al.* Evidence for a small hole pocket in the fermi surface of underdoped YBa2Cu3Oy. *Nat. Commun.* **6**, 6034 (2015).

53. Sebastian, S. E. *et al.* Fermi-liquid behavior in an underdoped high-T_c superconductor. *Phys. Rev. B* **81**, 140505 (2010).

54. Lee, P., Nagaosa, N. & Wen, X. Doping a mott insulator: physics of high-temperature superconductivity. *Rev. Mod. Phys.* **78**, 17–85 (2006).

55. Gurvitch, M. & Fiory, A. Resistivity of La1.825Sr0.175CuO4 and YBa2Cu3O7 to 1100 k: absence of saturation and its implications. *Phys. Rev. Lett.* **59**, 1337 (1987).

56. Timusk, T. & Statt, B. The pseudogap in high-temperature superconductors: an experimental survey. *Rep. Prog. Phys.* **62**, 61–122 (1999).

57. Cooper, R. *et al.* Anomalous criticality in the electrical resistivity of La2-xSrxCuO4. *Science* **323**, 603–607 (2009).

58. Gerber, S. *et al.* Three-dimensional charge density wave order in YBa2Cu3O6.67 at high magnetic fields. *Science* **350**, 949–952 (2015).

59. Yao, H., Lee, D. H. & Kivelson, S. Fermi-surface reconstruction in a smectic phase of a high-temperature superconductor. *Phys. Rev. B* **84**, 012507 (2011).

60. Andres, D., Kartsovnik, M. V., Grigoriev, P. D., Biberacher, W. & Müller, H. Orbital quantization in the high-magnetic-field state of a charge-density-wave system. *Phys. Rev. B* **68**, 201101 (2003).

61. Tabis, W. *et al.* Charge order and its connection with fermi-liquid charge transport in a pristine high-Tc cuprate. *Nat. Commun.* **5**, 5875 (2014).

62. Barišić′, N. *et al.* Universal quantum oscillations in the underdoped cuprate superconductors. *Nat. Phys.* **9**, 761–764 (2013).

63. Liang, R., Bonn, D. & Hardy, W. N. Preparation and x-ray characterization of highly ordered ortho-II phase YBa2Cu3O6.50 single crystals. *Phys. C: Superconductivity* **336**, 57–62 (2000).

64. Ramshaw, B. J. *et al.* Vortex lattice melting and H_{c2} in underdoped Yba$_2$Cu$_3$Oy. *Phys. Rev. B* **86**, 174501 (2012).

65. Peets, D. C. *et al.* Tl2Ba2CuO6+δ brings spectroscopic probes deep into the overdoped regime of the high-Tc cuprates. *New. J. Phys.* **9**, 28 (2007).